Acta Mech 227, 1799–1811 (2016)
DOI 10.1007/s00707-016-1597-2

ORIGINAL PAPER

Yin Yao · Shaohua Chen

Buckling behavior of nanowires predicted by a new surface energy density model

Received: 11 December 2015 / Revised: 29 January 2016 / Published online: 23 March 2016

Abstract The axial buckling behavior of nanowires is investigated with a new continuum theory, in which the surface effect of nanomaterials is characterized by the surface energy density. Only the surface energy density of bulk materials and the surface relaxation parameter are involved, instead of the surface elastic constants in the classical surface elasticity theory. Two kinds of nanowires with different boundary conditions are discussed. It is demonstrated that the new continuum theory can predict the buckling behavior of nanowires very well. Similar to the prediction of the classical elasticity theory, the critical compressive load of axial buckling of nanowires predicted by the new continuum theory increases with an increasing characteristic length, such as the diameter or height of nanowires. With the same aspect ratio, a nanowire with a rectangular cross section possesses a larger critical buckling load than that with a circular one. However, the surface effect could enhance the critical buckling load not only for a fixed–fixed nanowire but also for a cantilevered one in contrast to the classical elastic model. All the results predicted by the new continuum theory agree well with predictions by the surface elasticity models. The present research not only verifies the validation of the new continuum theory, but also gives a much more convenient characterization of buckling behaviors of nanowires. This should be helpful for the design of nanodevices based on nanomaterials, for example, nanobeams in NEMS or high-precision instruments.

1 Introduction

As a basic building component, nanowires have a wide range of potential applications in miniature devices, such as sensors, resonators and atomic force microscopy (AFM) tips [1–3]. In contrast to bulk materials, the elastic property of nanowires exhibits a distinct size-dependent behavior due to a large surface-to-volume ratio [4,5]. Both static and dynamic bending tests have been widely adopted in order to investigate the special mechanical feature of nanowires [6–11], in which it was found that the elastic modulus of a fixed–fixed nanowire increases, while that of a cantilevered one decreases with a decreasing characteristic length scale of nanowires. However, such a size (surface) effect cannot be predicted within the framework of the classical elasticity theory. New continuum theoretical models should be developed. Surface elasticity theory as an optional theory, which takes the surface effect into account [12,13], has been widely adopted to study the static and dynamic bending behaviors of nanowires successfully [14–17]. Molecular dynamics (MD) simulation method as a feasible numerical technique is also extensively used to investigate the size-dependent modulus of nanowires [18–21], besides the surface Cauchy–Born model [22] and the finite element calculation based on the surface elasticity theory [23].

Y. Yao · S. Chen (✉)
LNM, Institute of Mechanics, Chinese Academy of Sciences, Beijing 100190, China
E-mail: chenshaohua72@hotmail.com; shchen@LNM.imech.ac.cn
Tel.: 86-10-82543960
Fax: 86-10-82543977

Besides the bending behaviors of nanowires, during practical applications, for example, in nanodevices or nanoelectromechanical systems (NEMs), it is unavoidable for nanowires to sustain an axial compressive load, which, as a result, would induce buckling of nanowires [24–26].

Actually, many experiments about the buckling behavior of nanowires have been carried out. The critical buckling force of fixed–fixed zinc oxide (ZnO) nanowires is found to increase with an increasing nanowire radius [27,28]. A decreasing aspect ratio of a fixed–fixed silicon nanowire would induce an increasing critical buckling load [25]. The critical buckling force of a cantilevered silver-gallium alloy nanowire was measured by Dobrokhotov et al. [24]. MD calculations about the buckling behavior of nanowires were also done [26,29]. A common finding is that the critical buckling force measured experimentally is obviously larger than the prediction by the classical elasticity theory.

To precisely predict the critical buckling load of nanowires theoretically is an obviously significant problem. Consequently, surface elasticity beam models have been extended to analyze buckling of nanowires. Considering a nanowire as a composite system consisting of an elastic surface layer and a core part, Wang and Feng [30,31] proposed a core shell model and achieved closed-form solutions of the critical buckling force for both Euler and Timoshenko nanowires. Similar work was done by Yao and Yun [32] and Challamel and Elishakoff [33]. Chiu and Chen [17] introduced a surface flexural stiffness into the surface elasticity model to characterize the curvature-dependent surface energy of buckling nanowires. Juntarasaid et al. [34] carried out the buckling analysis considering effects of both surface elasticity and nonlocal elasticity. Wang et al. [35] analyzed effects of the surface elasticity and the residual surface tension on the in-plane buckling behavior of nanowires on elastomeric substrates.

Almost all of the above analyses on the critical buckling force are based on the surface elasticity model, which depends significantly on the surface elastic constants [17,30,36]. An open question of how to achieve the surface elastic constants still exists. No experiment technique is available to measure the surface elastic constants of nanomaterials. MD simulation is the only method to provide the constants [37–39], which are, however, inevitably influenced by several numerical aspects, including how to choose a proper atomic potential, how to choose the size of the numerical model and how many atom layers can be regarded as the surface of nanomaterials. Furthermore, a negative surface modulus adopted in the buckling analysis of metal nanowires was regarded as an ambiguous choice [16,17]. In the core–shell model [30,31], the surface elastic modulus was defined as a product of the bulk modulus and the thickness of the surface layer. How to determine the thickness of the surface layer still needs further investigations.

A new elasticity theory for nanomaterials and nanostructures has been developed recently [40], which provides an alternative way to account for the surface effect at nanoscales [41–43]. In the new theory, the surface of nanomaterials is also regarded as a zero-thickness layer. However, a surface-induced traction as a function of the surface-free energy density is introduced to characterize the surface effect. The involved parameters are only the bulk surface energy density (surface energy density of bulk materials) and the surface relaxation parameters induced by the self-relaxation of nanomaterials, instead of the surface elastic constants in the classical surface elasticity theory. Both parameters are easy to find in material handbooks or MD simulations [40,44].

The buckling behavior of nanowires is investigated in this paper using the new developed theory. One of the aims is to verify whether the new theoretical model is reasonable to predict the buckling behavior of nanowires. The other one is to achieve a closed-form solution of the critical buckling load, which may be more convenient for applications. The remainder of this paper is organized as follows. The new theory is briefly introduced first. Both the surface effects of the buckling behavior in nanowires with a fixed–fixed boundary condition and those with a cantilevered one are analyzed theoretically in Sect. 3. Discussions of the present results and comparisons with the existing theoretical and MD predictions are given in Sect. 4. Conclusions are finally provided in Sect. 5.

2 Brief introduction of the new theory for nanomaterials

A new continuum theory for nanomaterials was developed recently by Chen and Yao [40], in which nanosolids with idealized crystal structures are considered with three kinds of configurations, i.e., an initial one without deformation, an intermediate one after the self-relaxation of nanomaterials and a current one subjected to an external loading as shown in Fig. 1. A Lagrangian coordinate system is embedded in the surface and attached to the atoms [45], where a_{01} and a_{02} represent the initial lattice lengths parallel to the two basic vectors of the surface unit cell, and β denotes an angle between the two basic vectors. Due to the surface relaxation, the lattice

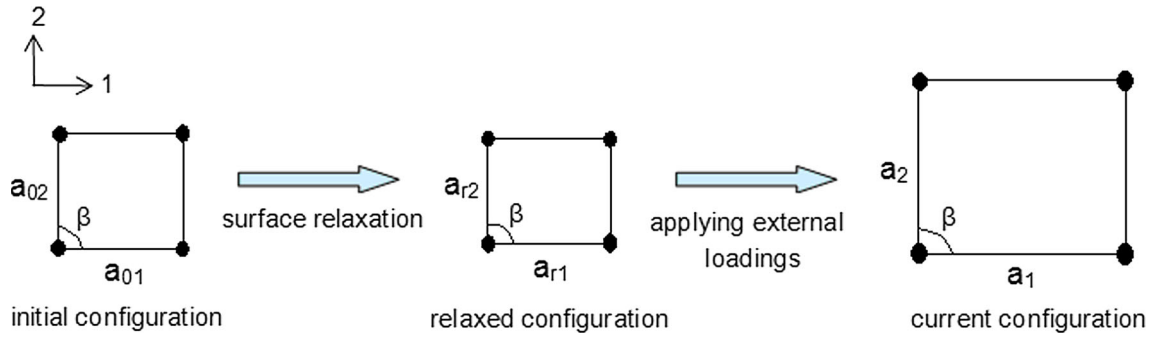

Fig. 1 Schematic of a surface unit cell in the initial (reference), relaxed (intermediate) and current configuration. Due to the self-relaxation and the external loading, the initial lattice constants a_{0i} $(i = 1, 2)$ become a_i $(i = 1, 2)$ through a_{ri} $(i = 1, 2)$

lengths become a_{r1} and a_{r2}, which further become a_1 and a_2 in the current configuration under an external loading. The Lagrangian surface energy density ϕ_0 with regard to the initial (reference) configuration can be divided into a structural part ϕ_0^{stru} related to the surface strain energy and a chemical part ϕ_0^{chem} originating from the surface dangling-bond energy,

$$\begin{aligned}
\phi_0 &= \phi_0^{\text{stru}} + \phi_0^{\text{chem}},\\
\phi_0^{\text{stru}} &= \frac{E_b}{2\sin\beta}\sum_{i=1}^{2} a_{0i}\eta_i\{[3+(\lambda_i+\lambda_i\varepsilon_{si})^{-m}-3(\lambda_i+\lambda_i\varepsilon_{si})]\\
&\quad \left[\lambda_i^2\varepsilon_{si}^2+(\lambda_i-1)^2+2\lambda_i(\lambda_i-1)\varepsilon_{si}\right]\},\\
\phi_0^{\text{chem}} &= \phi_{0b}\left(1-w_1\frac{D_0}{D}\right),\ \eta_1 = a_{01}/a_{02},\ \eta_2 = a_{02}/a_{01}
\end{aligned} \tag{1}$$

where ϕ_{0b} is the bulk surface energy density and D_0 is a critical size ($D_0 = 3d_a$ for nanoparticles and nanowires, $D_0 = 2d_a$ for nanothin films, where d_a is the atomic diameter). D is a characteristic scale of nanomaterials (e.g., height, diameter). w_1 is a parameter governing the size-dependent behavior of ϕ_0^{chem}. E_b is Young's modulus of a bulk material. $\lambda_i = a_{ri}/a_{0i}$ denotes the surface relaxation parameter, and $\varepsilon_{si} = (a_i - a_{ri})/a_{ri}$ is the surface strain induced only by the external loading. m is a parameter describing the dependence of bond lengths on the binding energy ($m = 4$ for alloys or compounds and $m = 1$ for pure metals) [46].

For nanomaterials, the total potential energy Π in the current configuration can be expressed as

$$\Pi(\boldsymbol{u}) = \int_{V-S}\psi(\boldsymbol{\varepsilon})\mathrm{d}V + \int_S \phi\mathrm{d}S - \int_{V-S}\boldsymbol{f}\cdot\boldsymbol{u}\mathrm{d}V - \int_{S_p}\boldsymbol{p}\cdot\boldsymbol{u}\mathrm{d}S \tag{2}$$

where ψ is the elastic strain energy density in the bulk and the second term at the right of Eq. (2) is the surface energy of nanomaterials. ϕ is the Eulerian surface energy density in the current configuration. $\boldsymbol{f}$ and $\boldsymbol{p}$ denote the body force and the external surface traction, respectively. $\boldsymbol{u}$ and $\boldsymbol{\varepsilon}$ are the displacement and the strain induced by $\boldsymbol{f}$ and $\boldsymbol{p}$. Variation analysis of Eq. (2) yields the equilibrium equations and the stress boundary conditions of nanosolids,

$$\begin{aligned}
&\boldsymbol{\sigma}\cdot\nabla + \boldsymbol{f} = 0 \quad (\text{in}V - S),\\
&\boldsymbol{n}\cdot\boldsymbol{\sigma}\cdot\boldsymbol{n} = \boldsymbol{p}\cdot\boldsymbol{n} - \gamma_n\boldsymbol{n} \quad (\text{on}S),\\
&(\boldsymbol{I}-\boldsymbol{n}\otimes\boldsymbol{n})\cdot\boldsymbol{\sigma}\cdot\boldsymbol{n} = (\boldsymbol{I}-\boldsymbol{n}\otimes\boldsymbol{n})\cdot\boldsymbol{p} - \boldsymbol{\gamma}_t \quad (\text{on } S)
\end{aligned} \tag{3}$$

where $\boldsymbol{\sigma}$ is the bulk Cauchy stress tensor, $\boldsymbol{n}$ is the unit normal vector perpendicular to the boundary surface S of the nanosolid, $\boldsymbol{I}$ is a unit tensor; γ_n and $\boldsymbol{\gamma}_t$ are the normal and tangential components of a surface-induced traction vector, respectively, which characterize the force disturbance at boundaries due to the surface effect. Based on an infinitesimal element, the virtual work method yields the surface-induced traction, which is related to the Eulerian surface energy density [40] by

$$\boldsymbol{\gamma}_t = \nabla_s\phi,\ \gamma_n\boldsymbol{n} = \phi\left(\frac{1}{R_1}+\frac{1}{R_2}\right)\boldsymbol{n} = \phi\,(\boldsymbol{n}\cdot\nabla_s)\,\boldsymbol{n} \tag{4}$$

where ∇_s is a surface gradient operator, and R_1 and R_2 are the two principal radii of curvature of a curved surface.

According to Chen and Yao [40], Nix and Gao [45] and Huang and Wang [47], the Eulerian surface energy density ϕ in the current configuration is related to the Lagrangian surface energy density ϕ_0 by

$$\phi = \frac{\phi_0}{J_s} \tag{5}$$

where J_s is a Jacobian determinant characterizing the surface deformation from the reference configuration to the current one.

Substituting Eqs. (4) and (5) into Eq. (3) yields the governing equations in terms of the Lagrangian surface energy density,

$$\begin{aligned} &\boldsymbol{\sigma}\cdot\nabla+\boldsymbol{f}=0 \quad (\text{in } V-S),\\ &\boldsymbol{n}\cdot\boldsymbol{\sigma}\cdot\boldsymbol{n}=\boldsymbol{p}\cdot\boldsymbol{n}-\frac{\phi_0(\boldsymbol{n}\cdot\nabla_s)}{J_s} \quad (\text{on } S),\\ &(\boldsymbol{I}-\boldsymbol{n}\otimes\boldsymbol{n})\cdot\boldsymbol{\sigma}\cdot\boldsymbol{n}=(\boldsymbol{I}-\boldsymbol{n}\otimes\boldsymbol{n})\cdot\boldsymbol{p}+\frac{\phi_0(\nabla_s J_s)}{J_s^2}-\frac{\nabla_s\phi_0}{J_s} \quad (\text{on } S). \end{aligned} \tag{6}$$

In contrast to the G–M theory [12], the advantage of the new theory is that the surface elastic constants are no longer required. The Lagrangian surface energy density ϕ_0 serves as a unique quantity characterizing the surface effect of nanomaterials, which depends only on the bulk surface energy density and the relaxation parameter [40]. Both parameters have clear physical meanings and are very easy to be determined through material handbooks and simple MD simulations.

3 Surface effect in buckling nanowires

As shown in Fig. 2, a nanowire buckles due to an axially compressive load P larger than the critical buckling one P_{cr}. Two kinds of boundary conditions, i.e., a cantilevered nanowire beam and a fixed–fixed one, are investigated as shown in Fig. 2a, b. Here, the fixed–fixed nanowire can be regarded as a beam with a clamped end and a slidingly hinged one [48]. The length of the nanowire in the x direction is L with a vertical deflection in the z direction. The cross section of the nanowire is rectangular with a height h and a width $b(b \geq h)$, or circular with a diameter d as shown in Fig. 2c.

3.1 Deflection equation of nanowires

When buckling occurs, the nanowire will deflect. u_x, u_z and ε_x denote the axial displacement, the vertical displacement, and the axial strain of the buckling nanowire, respectively, which can be obtained with the assumption of Euler–Bernoulli beam as [48]

$$u_x = -z\frac{\mathrm{d}w}{\mathrm{d}x}, \quad \varepsilon_x = -z\frac{\mathrm{d}^2w}{\mathrm{d}x^2}, \quad u_z = w(x), \quad 0 \leq x \leq L. \tag{7}$$

For simplicity, consider a [100] axially oriented nanowire with a symmetrically lateral surface and an equal atom spacing in both bond directions, e.g., the (001) or (010) surface [15,16,30]. Therefore, the Lagrangian surface energy density can be written as [40,42,43]

$$\phi_0 = \phi_{0b}\left(1-\frac{3d_a}{4D}\right)+\frac{\sqrt{2}E_b a_0}{2}\left[3+\frac{1}{\lambda\,(1+\varepsilon_x/2)}-3\left(\lambda+\frac{\lambda\varepsilon_x}{2}\right)\right]\left[\frac{\lambda^2\varepsilon_x^2}{4}+2\lambda(\lambda-1)\frac{\varepsilon_x}{2}+(\lambda-1)^2\right] \tag{8}$$

where λ and a_0 represent the surface relaxation parameter in both bond directions of the (001) surface and the bulk lattice constant, respectively; D is the diameter or height of nanowires.

The variation of the bulk strain energy is written as

$$\delta U = \delta\int_V \frac{1}{2}\sigma_x\varepsilon_x \mathrm{d}V = \delta\int_0^L \frac{1}{2}E_b I\left(\frac{\mathrm{d}^2w}{\mathrm{d}x^2}\right)^2\mathrm{d}x = \int_0^L E_b I\frac{\mathrm{d}^2w}{\mathrm{d}x^2}\frac{\mathrm{d}^2(\delta w)}{\mathrm{d}x^2}\mathrm{d}x \tag{9}$$

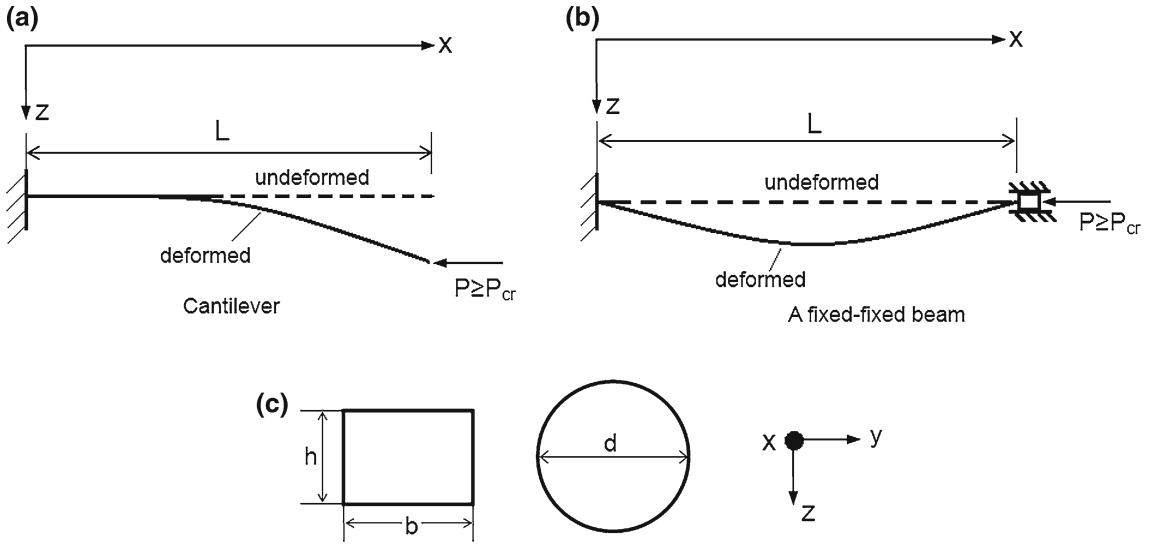

Fig. 2 Schematic of a nanowire with different boundary conditions under an externally compressive load P. **a** A cantilevered nanowire; **b** a fixed–fixed nanowire; **c** the cross section of the nanowire, one is *rectangular* and the other is *circular*

where $I = \int_{A_{nw}} z^2 \mathrm{d}A$ is the inertia moment and A_{nw} denotes the nanowire's cross section, and E_b is Young's modulus of bulk materials.

The variation of the surface energy can be written as [49]

$$\delta\Phi = \int_{S_{nw}} \boldsymbol{\gamma} \cdot \delta\boldsymbol{u} \mathrm{d}S = \int_0^L \mathrm{d}x \int_{C_{nw}} (\gamma_x \delta u_x + \gamma_n \delta u_n) \mathrm{d}C \tag{10}$$

where S_{nw} represents the surface of nanowires, C_{nw} is the perimeter of a rectangular or circular cross section. γ_x and γ_n represent the axial and normal components of the surface-induced traction, respectively. δu_x and δu_n are the corresponding displacement components of $\delta\boldsymbol{u}$. Combining Eqs. (4), (5), (7), and (8) and noting that $J_s = \lambda^2(1+\varepsilon_x/2)^2$ yield the axial surface-induced traction γ_x [42,43],

$$\begin{aligned}
\gamma_x &= \left[C_0 z + C_1 z^2 \frac{\mathrm{d}^2 w}{\mathrm{d}x^2} + C_2 z^3 \left(\frac{\mathrm{d}^2 w}{\mathrm{d}x^2} \right)^2 \right] \frac{\mathrm{d}^3 w}{\mathrm{d}x^3}, \\
C_0 &= \phi_0^*(5-4\lambda) - \frac{\sqrt{2} E_b a_0 A_2 (3-2\lambda)}{2}, \\
C_1 &= 2\phi_0^* + \sqrt{2} E_b a_0 A_1 (3-2\lambda) - \frac{\sqrt{2} E_b a_0 A_2 (5-4\lambda)}{2}, \\
C_2 &= \frac{\sqrt{2} E_b a_0 A_1 (7-4\lambda)}{2} - \sqrt{2} E_b a_0 A_2, \quad \phi_0^* = \phi_{0b} \left(1 - \frac{3 d_a}{4D} \right) + \frac{\sqrt{2} E_b a_0}{2} (\lambda - 1)^2, \\
A_1 &= \frac{1 - 10(\lambda-1) - 17(\lambda-1)^2}{4}, \quad A_2 = (\lambda-1) - 5(\lambda-1)^2.
\end{aligned} \tag{11}$$

Noting the curvature $\kappa = -(\boldsymbol{n} \cdot \nabla_s) = \mathrm{d}^2 w / \mathrm{d}x^2$ and $\delta u_n \approx \delta w$[16,50], the variation of the energy induced by the normal surface-induced traction γ_n can be expressed as

$$\begin{aligned}
\gamma_n \delta u_n \approx -\phi \kappa \delta w &= -\left[D_0 z + D_1 z \frac{\mathrm{d}^2 w}{\mathrm{d}x^2} + D_2 z^2 \left(\frac{\mathrm{d}^2 w}{\mathrm{d}x^2} \right)^2 + D_3 z^3 \left(\frac{\mathrm{d}^2 w}{\mathrm{d}x^2} \right)^3 \right] \frac{\mathrm{d}^2 w}{\mathrm{d}x^2} \delta w, \\
D_0 &= \phi_0^*(3-2\lambda), \quad D_1 = \phi_0^* - \frac{\sqrt{2} E_b a_0 A_2 (3-2\lambda)}{2}, \\
D_2 &= \frac{\sqrt{2} E_b a_0 A_1 (3-2\lambda)}{2} - \sqrt{2} E_b a_0 A_2, \quad D_3 = \frac{\sqrt{2} E_b a_0 A_1}{2}.
\end{aligned} \tag{12}$$

With a small deformation assumption, the work done by the compressive load can be written as [48]

$$W_p = P\left[L - \int_0^L \mathrm{d}s\right] = P\left[L - \int_0^L \frac{\mathrm{d}x}{\sqrt{1+(\mathrm{d}z/\mathrm{d}x)^2}}\right] \approx \frac{P}{2}\int_0^L \left(\frac{\mathrm{d}w}{\mathrm{d}x}\right)^2 \mathrm{d}x. \tag{13}$$

Based on Eqs. (9)–(13), the variation of the potential energy is obtained,

$$\begin{aligned}\delta\Pi &= \delta U + \delta\Phi - \delta W_p \\ &= \int_0^L E_b I \frac{\mathrm{d}^2 w}{\mathrm{d}x^2}\frac{\mathrm{d}^2(\delta w)}{\mathrm{d}x^2}\mathrm{d}x - \int_0^L \left[C_0 I_{s1} + C_2 I_{s2}\left(\frac{\mathrm{d}^2 w}{\mathrm{d}x^2}\right)^2\right]\frac{\mathrm{d}^3 w}{\mathrm{d}x^3}\frac{d(\delta w)}{\mathrm{d}x}\mathrm{d}x \\ &\quad - \int_0^L \left[D_0 I_c + D_2 I_{s1}\left(\frac{\mathrm{d}^2 w}{\mathrm{d}x^2}\right)^2\right]\frac{\mathrm{d}^2 w}{\mathrm{d}x^2}\delta w\mathrm{d}x - \int_0^L P\frac{\mathrm{d}w}{\mathrm{d}x}\frac{\mathrm{d}(\delta w)}{\mathrm{d}x}\mathrm{d}x\end{aligned} \tag{14}$$

where $I_{s1} = \int_{C_{NW}} z^2 \mathrm{d}C$, $I_{s2} = \int_{C_{NW}} z^4 \mathrm{d}C$ and $I_c = \int_{C_{nw}} n_w^2 \mathrm{d}C$. Here, n_w represents the vertical component of the unit normal vector $\boldsymbol{n}$, which is parallel to $w(x)$.

With regard to cross sections of different shapes, we have

$$\begin{aligned}\text{Rectangular: } I &= \frac{bh^3}{12}, \quad I_{s1} = \frac{bh^2}{2} + \frac{h^3}{6}, \quad I_{s2} = \frac{bh^4}{8} + \frac{h^5}{80}, \quad I_c = 2b, \\ \text{Circular: } I &= \frac{\pi d^4}{64}, \quad I_{s1} = \frac{\pi d^3}{8}, \quad I_{s1} = \frac{3\pi d^5}{128}, \quad I_c = \frac{\pi d}{2}.\end{aligned} \tag{15}$$

Ignoring high-order terms yields

$$\begin{aligned}\delta\Pi &= \int_0^L (E_b I + C_0 I_{s1})\frac{\mathrm{d}^4 w}{\mathrm{d}x^4}\delta w\mathrm{d}x + \int_0^L (P - D_0 I_c)\frac{\mathrm{d}^2 w}{\mathrm{d}x^2}\delta w\mathrm{d}x \\ &\quad + \left[E_b I\frac{\mathrm{d}^2 w}{\mathrm{d}x^2}\frac{\mathrm{d}(\delta w)}{\mathrm{d}x}\right]_{x=0}^{x=L} - \left\{\left[(E_b I + C_0 I_{s1})\frac{\mathrm{d}^3 w}{\mathrm{d}x^3} + P\frac{\mathrm{d}w}{\mathrm{d}x}\right]\delta w\right\}_{x=0}^{x=L}.\end{aligned} \tag{16}$$

Then, letting $\delta\Pi = 0$ yields the deflection equation and the boundary conditions,

$$\begin{aligned}&(E_b I + C_0 I_{s1})\frac{\mathrm{d}^4 w}{\mathrm{d}x^4} + (P - D_0 I_c)\frac{\mathrm{d}^2 w}{\mathrm{d}x^2} = 0, \\ &\left[E_b I\frac{\mathrm{d}^2 w}{\mathrm{d}x^2}\frac{\mathrm{d}(\delta w)}{\mathrm{d}x}\right]_{x=0}^{x=L} = 0, \quad \left\{\left[(E_b I + C_0 I_{s1})\frac{\mathrm{d}^3 w}{\mathrm{d}x^3} + P\frac{\mathrm{d}w}{\mathrm{d}x}\right]\delta w\right\}_{x=0}^{x=L} = 0.\end{aligned} \tag{17}$$

It is interesting to find that the deflection equation in (17) has an analogous form to that derived by the surface elasticity models [30,33]. However, the terms characterizing the surface effect $C_0 I_{s1}$ and $D_0 I_c$ do not contain any surface elastic constants. For wires (beams) with relatively large scales, we have $C_0 = 0$ and $D_0 = 0$. The deflection equation is well degraded to the classical one without the surface effect, i.e., $E_b I w^{(4)}(x) + P w''(x) = 0$ [48].

3.2 The critical buckling load

3.2.1 The case of a fixed–fixed nanowire

Solving Eq. (17) yields the general solution of the deflection function $w(x)$,

$$\begin{aligned}w(x) &= S_1 + S_2 x + S_3\cos(kx) + S_4\sin(kx), \\ k &= \sqrt{\frac{P - D_0 I_c}{E_b I + C_0 I_{s1}}}, \quad 0 \le x \le L,\ P > D_0 I_c\end{aligned} \tag{18}$$

where $S_1 \sim S_4$ are unknown coefficients. The boundary conditions of a fixed–fixed buckling nanowire are

$$\begin{aligned} x = 0: \quad & w = 0, \quad \frac{\mathrm{d}w}{\mathrm{d}x} = 0, \\ x = L: \quad & w = 0, \quad \frac{\mathrm{d}w}{\mathrm{d}x} = 0. \end{aligned} \tag{19}$$

Combining Eqs. (18) and (19) leads to the governing equation with respect to the compressive load P,

$$\cos\left(\sqrt{\frac{P - D_0 I_c}{E_b I + C_0 I_{s1}}} L\right) = 1 \tag{20}$$

which further gives

$$\frac{P - D_0 I_c}{E_b I + C_0 I_{s1}} = \frac{4n^2\pi^2}{L^2}, \quad n = 1, 2, 3, \ldots \tag{21}$$

Letting $n = 1$, one can find the critical buckling load P_{cr} of fixed–fixed nanowires,

$$P_{cr} = \frac{4\pi^2 (E_b I + C_0 I_{s1})}{L^2} + D_0 I_c. \tag{22}$$

The critical buckling load in Eq. (22) can be well reduced to the solution predicted by the classical elasticity theory only when the characteristic length of wires is large enough [48], i.e.,

$$P_{cr}^0 = \frac{4\pi^2 E_b I}{L^2}. \tag{23}$$

It is very obvious to find that the critical buckling load predicted by the present model should be larger than that achieved by the classical elasticity theory. That is to say, the classical theory without considering the surface effect would underestimate the critical buckling load of nanowires.

3.2.2 The case of a cantilevered nanowire

The general solution of the deflection function $w(x)$ in Eq. (18) is also fit for the case of cantilevered nanowires as shown in Fig. 2a, but with different boundary conditions,

$$\begin{aligned} x = 0: \quad & w = 0, \quad \frac{\mathrm{d}w}{\mathrm{d}x} = 0, \\ x = L: \quad & E_b I \left(\frac{\mathrm{d}^2 w}{\mathrm{d}x^2}\right) = 0, \quad (E_b I + C_0 I_{s1}) \frac{\mathrm{d}^3 w}{\mathrm{d}x^3} + P \frac{\mathrm{d}w}{\mathrm{d}x} = 0. \end{aligned} \tag{24}$$

Combining Eqs. (18) and (24) yields a transcendental equation with respect to P,

$$\cos\left(\sqrt{\frac{P - D_0 I_c}{E_b I + C_0 I_{s1}}} L\right) = \frac{D_0 I_c}{P} \tag{25}$$

which is analogous to the following equation based on the surface elasticity theory [33]:

$$\cos\left(\sqrt{\frac{P - 2\tau_0 D}{E_b I + E_s I_{s1}}} L\right) = \frac{2\tau_0 D}{P}. \tag{26}$$

E_s and τ_0 are the surface elastic modulus and surface residual tension, respectively [33]. D represents a characteristic length of nanowires (diameter or height).

The smallest solution of Eq. (25) within $P > D_0 I_c$ can be numerically solved, which is referred to as the critical buckling load of cantilevered nanowires. Equation (25) would be reduced to the equation $\cos(\sqrt{P/E_b I} L) = 0$ predicted by the classical beam theory when the wire (beam) owns a relatively large characteristic scale. As a result, the critical buckling load for a cantilevered beam obtained by the classical beam theory is $P_{cr}^0 = \pi^2 E_b I / 4L^2$[48].

4 Results and discussion

The critical buckling loads in Eqs. (22) and (25) for a fixed–fixed nanowire and a cantilevered one will be analyzed, respectively, for typical nanowires. The material parameters for a silver nanowire can be found from Sheng et al. [51] with $d_a = 0.2889\,\text{nm}$, $a_0 = 0.418\,\text{nm}$, $E_b = 78\,\text{GPa}$, $\phi_{0b(001)} = 1.2\,\text{J/m}^2$. For simplicity, let the rectangular nanowire have a square cross section, i.e., $b = h$. Then the surface relaxation parameter λ is proportional to the height or diameter of nanowires, which has been expressed as $\lambda = 1 - c_r/D$ ($c_r > 0$, $D = h$ or d) [26,40,52] with $c_r \approx 0.016\,\text{nm}$ for the (001) surface of Ag [40]. One can see that λ tends to be unity when the characteristic length is relatively large, for example $D \geq 5\,\text{nm}$. Comparatively, in the theoretical analysis with the surface elasticity theory, the involved surface elastic modulus and the surface residual tension of Ag nanowires were taken as $E_s = 1.2\,\text{N/m}$ and $\tau_0 = 0.89\,\text{N/m}$, respectively [30].

The critical buckling load of Ag nanowires with a circular cross section but two different boundary conditions is given in Fig. 3a, b as a function of the diameter of the nanowires, respectively, where not only the result predicted by the new model but also the one achieved by the surface elasticity theory is shown. The prediction of the classical beam theory is further exhibited for comparison. It is found that the present result predicted

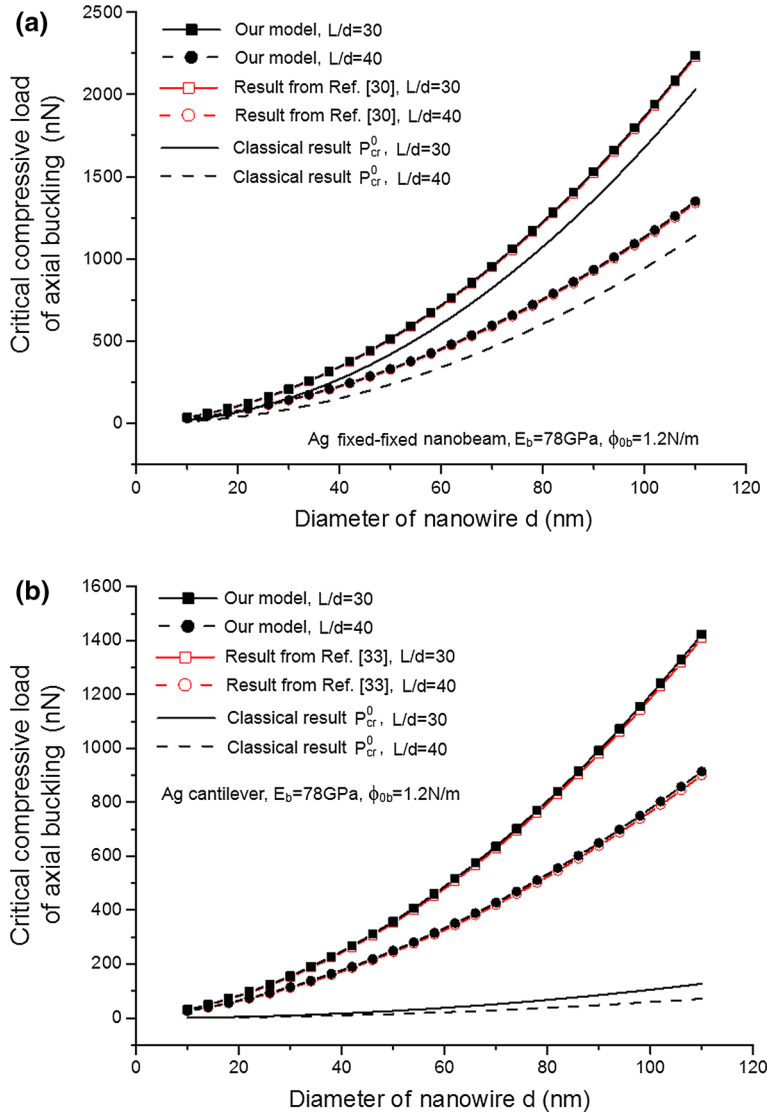

Fig. 3 The critical buckling load predicted by the present model, the surface elasticity one and the classical ones [30,33] as a function of the diameter of Ag nanowires with different aspect ratios and boundary conditions. **a** For a fixed–fixed nanowire; **b** for a cantilevered one

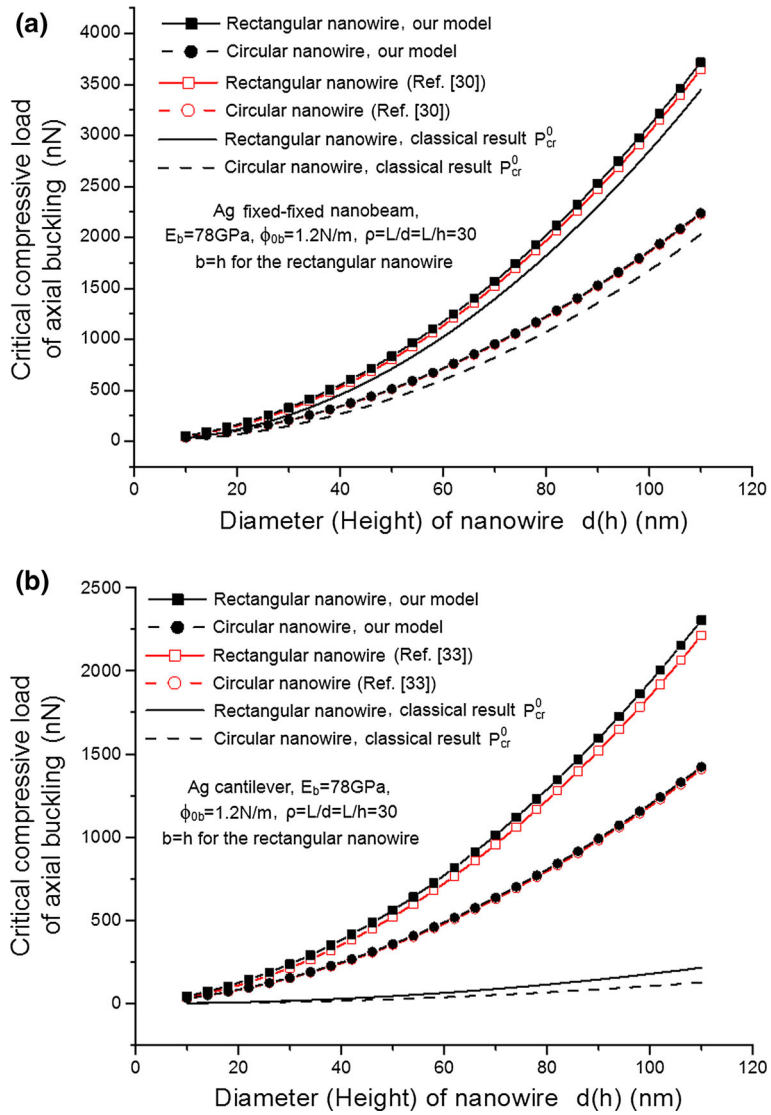

Fig. 4 The normalized critical buckling load P_{cr}/P_{cr}^0 predicted by the present model, the surface elasticity ones [30,33] and the classical one as a function of the characteristic length (diameter or height) of Ag nanowires with different boundary conditions. **a** For a fixed–fixed nanowire; **b** for a cantilevered one

by the new model agrees very well with the ones predicted by the surface elasticity theory models [30,33]. Without loss of generality, the critical buckling load predicted by all the models with or without the surface effect increases with an increasing diameter or a decreasing aspect ratio of nanowires. However, the critical buckling load predicted by models considering the surface effect is obviously larger than that predicted by the classical beam theory not only for the fixed–fixed nanowire but also for the cantilevered one. It means that the critical buckling load of nanowires may be underestimated without considering the surface effect. That is to say, the surface effect in nanowires may improve their resistance to buckling.

The shape effect of the nanowires' cross section on the critical buckling load is studied and shown in Fig. 4, where the results for a fixed–fixed boundary case and a cantilevered one are given in Fig. 4a, b, respectively. With the same aspect ratio for nanowires with a rectangular cross section and a circular one, an obvious finding is that the critical buckling load of nanowires with a rectangular cross section is significantly larger than that with a circular cross section not only for fixed–fixed nanowires but also for cantilevered ones. Both the present model and the surface elasticity theory model could give such a conclusion. Furthermore, the critical buckling load predicted by the models considering the surface effect agrees well with the other ones not only for the

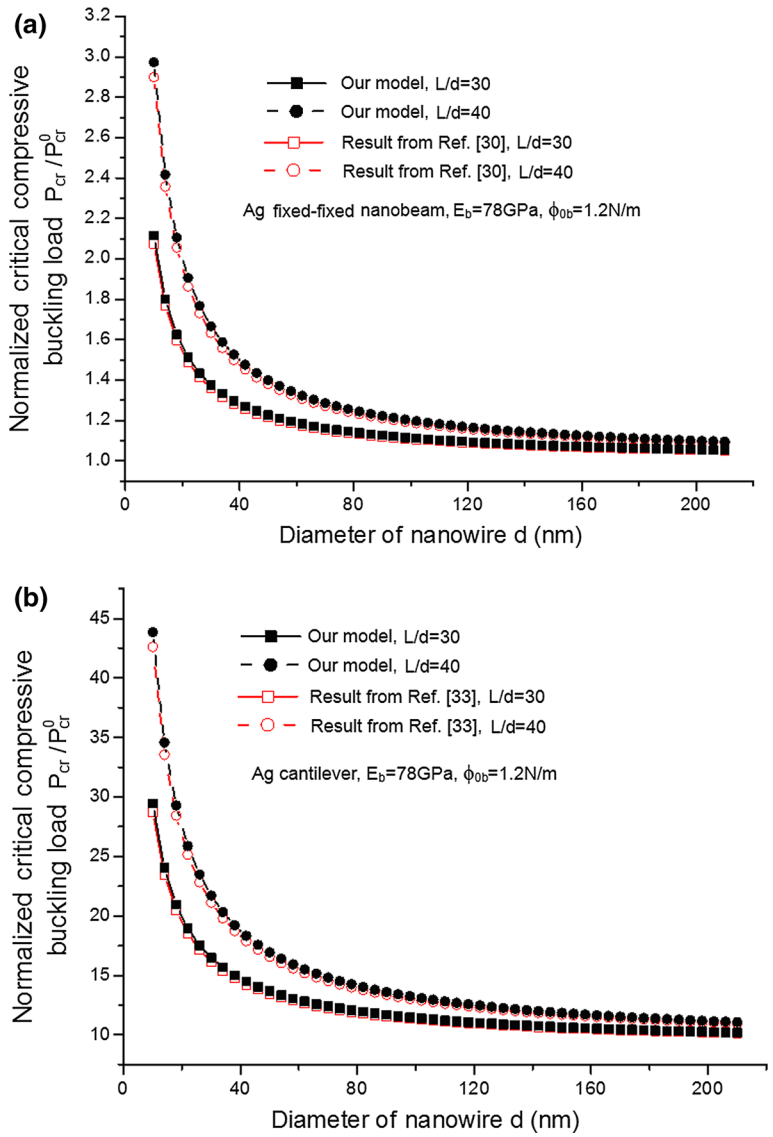

Fig. 5 Comparison of the normalized critical buckling load P_{cr}/P_{cr}^0 as a function of the diameter of Ag nanowires predicted by the present model and the surface elasticity ones [30,33]. **a** For a fixed–fixed nanowire; **b** for a cantilevered one

rectangular cross-sectional case but also for the circular one, which, however, is larger than that achieved by the classical beam theory.

To investigate the surface effect on the critical buckling load, we normalize the critical buckling load predicted by the models considering the surface effect with the one predicted by the classical theory, i.e., P_{cr}/P_{cr}^0, which is shown in Fig. 5a, b as a function of the diameter of nanowires for fixed–fixed Ag nanowires and cantilevered ones, respectively. The results obtained by the surface elasticity theory models are also given for comparison [30,33]. It shows that the surface effect on the critical buckling load of nanowires is weakened with an increasing characteristic length (diameter) or a decreasing aspect ratio for both the fixed–fixed nanowire case and the cantilevered one. Comparing both cases yields that the surface effect in cantilevered nanowires can be found at a much larger characteristic length (diameter) than that in fixed–fixed ones. Interestingly, such a phenomenon was also found experimentally by Dobrokhotov et al. [24] for a Silver-Gallium alloy (Ag_2Ga) cantilevered nanowire with a submicron diameter $d = 157\,\text{nm}$ and a length $L = 15.6\,\mu\text{m}$, in which the critical buckling load was measured to be about 200 nN, almost ten times higher than the classical prediction $P_{cr}^0 = 20.36\,\text{nN}$ [24]. However, quantitative comparison between the theoretical and experimental predictions cannot be carried out now due to the unavailable alloy material parameters. Experiments on the buckling

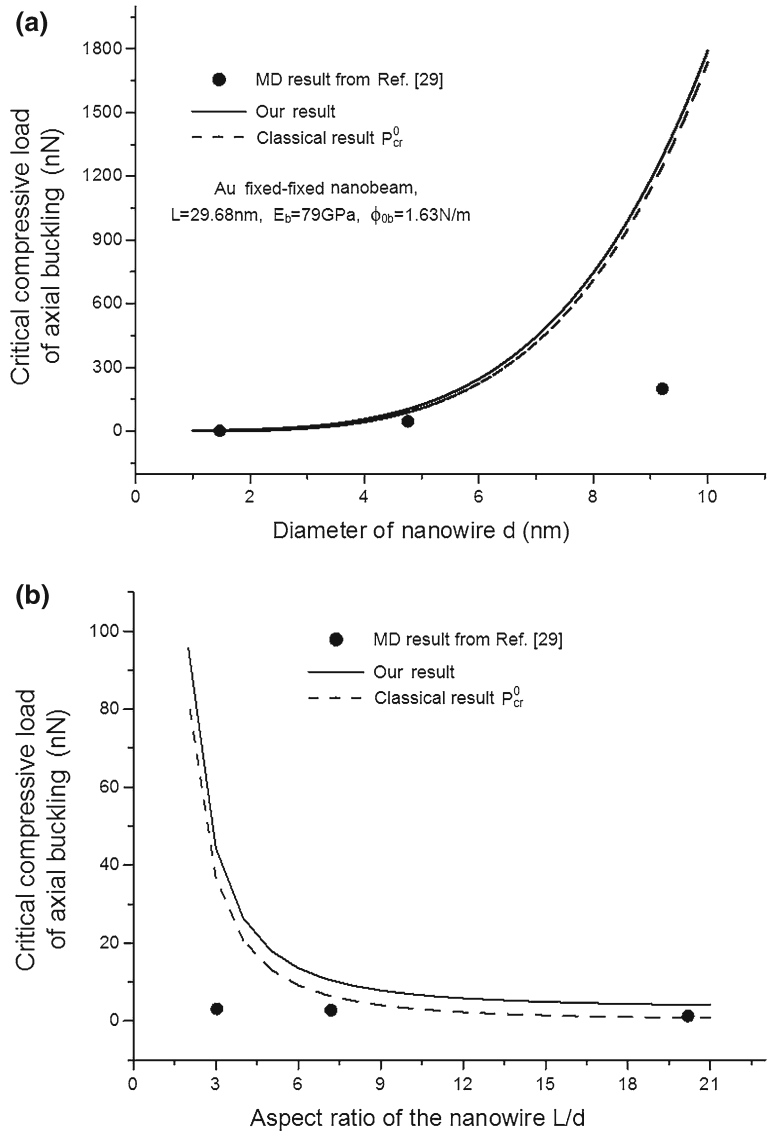

Fig. 6 Comparison of the critical buckling load predicted by the present model, the classical one and MD simulations [29] for Au nanowires as a function of **a** the diameter and **b** the aspect ratio

behavior of a simple metal need to be done in the future, which may be very useful for further checking the theoretical results.

Figure 6a, b gives the critical buckling load as a function of the diameter and the aspect ratio of fixed–fixed gold nanowires, respectively, in which not only the result predicted by the present model but also those given by the classical elasticity one and MD simulation [29] is shown for comparison. The material parameters involved in the present model are taken as $d_a = 0.2884\,\text{nm}$, $a_0 = 0.42\,\text{nm}$, $E_b = 79\,\text{GPa}$, $\phi_{0b(001)} = 1.63\,\text{J/m}^2$, $c_r \approx 0.025\,\text{nm}$ [40,51]. It is found that the theoretical predictions agree well with the numerical one only when the diameter is relatively small ($d \leq 5\,\text{nm}$) or the aspect ratio is relatively large ($\rho \geq 7$). From the above, we know that the critical buckling load would increase if the diameter of nanowires increases or the aspect ratio decreases. As a result, the critical buckling load may exceed the yield plasticity limit of nanowires, leading to irreversible plastic deformation, such as surface reconstruction, crystal twins and partial dislocations [29]. Energy dissipation and a reduction in load-bearing capacity should occur [53], resulting in a much lower critical buckling load than the theoretical prediction with an assumption of perfect elasticity.

5 Conclusions

The buckling behavior of nanowires subjected to a compressive load is analyzed in this paper using a recently developed elastic continuum model [40]. Two kinds of boundary conditions, i.e., a fixed–fixed one and a cantilevered one, are considered. The buckling equation is obtained as well as the critical buckling load. Comparison among the present theoretical prediction of the critical buckling load, the results given by the surface elasticity models [30,33] and the classical elasticity theory demonstrates that the surface effect in nanowires could improve the resistance of buckling, while the classical elastic theory would underestimate the critical buckling load of nanowires. No matter for nanowires with a fixed–fixed boundary condition or a cantilevered one, the critical buckling load increases with an increasing characteristic length (diameter or height) or a decreasing aspect ratio. The shape of the cross section can also show influence on the critical buckling load, and a rectangular one is found better than a circular one. This study can not only provide evidence of efficiency of the new developed model for predicting the buckling behavior of nanowires but also be helpful for the design of nanodevices with nanowires.

Acknowledgments The work reported here is supported by NSFC by Grants #11372317, #11125211, #11402270, the Nano-project (2012CB937500) and the CAS/SAFEA International Partnership Program for Creative Research Teams.

References

1. Craighead, H.G.: Nanoelectromechanical systems. Science **290**, 1532–1535 (2000)
2. Wu, B., Heidelberg, A., Boland, J.J.: Mechanical properties of ultrahigh-strength gold nanowires. Nat. Mater. **4**, 525–529 (2005)
3. Llobet, J., Sansa, M., Gerboles, M., Mestres, N., Arbiol, J., Borrise, X., Murano-Perez, F.: Enabling electromechanical transduction in silicon nanowire mechanical resonators fabricated by focused ion beam implantation. Nanotechnology **25**, 135302 (2014)
4. McDowell, M.T., Leach, A.M., Gall, K.: On the elastic modulus of metallic nanowires. Nano Lett. **8**, 3613–3618 (2008)
5. Wang, J.X., Huang, Z.P., Duan, H.L., Yu, S.W., Feng, X.Q., Wang, G.F., Zhang, W.X., Wang, T.J.: Surface stress effect in mechanics of nanostructured materials. Acta. Mech. Solida Sin. **24**, 52–82 (2011)
6. Cuenot, S., Fretigny, C., Champagne, S.D., Nysten, B.: Surface tension effect on the mechanical properties of nanomaterials measured by atomic force microscopy. Phys. Rev. B **69**, 165410 (2004)
7. Chen, Y.X., Dorgan, B.L., Mcllroy, D.N., Aston, D.E.: On the importance of boundary conditions on nanomechanical bending behavior and elastic modulus determination of silver nanowires. J. Appl. Phys. **100**, 104301 (2006)
8. Jing, G.Y., Duan, H.L., Sun, X.M., Zhang, Z.S., Xu, J., Li, Y.D., Wang, J.X., Yu, D.P.: Surface effects on elastic properties of silver nanowires: Contact atomic-force microscopy. Phys. Rev. B **73**, 235409 (2006)
9. Gavan, K.B., Westra, H.J.R., Vander drift, E.W.J.M., Venstra, W.J., Vander zant, H.S.J.: Surface effects on elastic properties of silver nanowires: Contact atomic-force microscopy. Appl. Phys. Lett. **94**, 233108 (2009)
10. Sadeghian, H., Yang, C.K., Goosen, J.F.L., Bossche, A., Staufer, U., French, P.J., Van Keulen, F.: Effects of size and defects on the elasticity of silicon nanocantilevers. Nanotechnology **20**, 064012 (2010)
11. Celik, E., Guven, I., Madenci, E.: Mechanical characterization of nickel nanowires by using a customized atomic force microscope. Nanotechnology **22**, 155702 (2011)
12. Gurtin, M.E., Murdoch, A.I.: A continuum theory of elastic material surfaces. Arch. Ration. Mech. Anal. **57**, 291–323 (1975)
13. Gurtin, M.E., Murdoch, A.I.: Surface stress in solids. Int. J. Solids Struct. **14**, 431–440 (1978)
14. Wang, G.F., Feng, X.Q.: Effects of surface elasticity and residual surface tension on the natural frequency of microbeams. Appl. Phys. Lett. **90**, 231904 (2007)
15. He, J., Lilley, C.M.: Surface Effect on the elastic behavior of static bending nanowires. Nano Lett. **8**, 1798–1802 (2008)
16. Song, F., Huang, G.L., Park, H.S., Liu, X.N.: A continuum model for the mechanical behavior of nanowires including surface and surface-induced initial stresses. Int. J. Solids Struct. **48**, 2154–2163 (2011)
17. Chiu, M.S., Chen, T.Y.: Effects of high-order surface stress on buckling and resonance behavior of nanowires. Acta Mech. **223**, 1473–1484 (2012)
18. Park, S.H., Kim, J.S., Park, J.H., Lee, J.S., Choi, Y.K., Kwon, O.M.: Molecular dynamics study on size-dependent elastic properties of silicon nanocantilevers. Thin Solid Films **492**, 285–289 (2005)
19. Chhapadia, P., Mohammadi, P., Sharma, P.: Curvature-dependent surface energy and implications for nanostructures. J. Mech. Phys. Solids **59**, 2103–2115 (2011)
20. Mohammadi, P., Sharma, P.: Atomistic elucidation of the effect of surface roughness on curvature dependent surface energy, surface stress, and elasticity. Appl. Phys. Lett. **100**, 133110 (2012)
21. Georgakaki, D., Ziogos, O.G., Polatoglou, H.M.: Vibrational and mechanical properties of Si/Ge nanowires as resonators: A molecular dynamics study. Phys. Status Solidi A **211**, 267–276 (2014)
22. Park, H.S., Klein, P.A.: Surface stress effects on the resonant properties of metal nanowires: The importance of finite deformation kinematics and the impact of the residual surface stress. J. Mech. Phys. Solids **56**, 3144–3166 (2008)
23. Feng, Y.K., Liu, Y.L., Wang, B.: Finite element analysis of resonant properties of silicon nanowires with consideration of surface effects. Acta Mech. **217**, 149–155 (2011)
24. Dobrokhotov, V.V., Yazdanpanah, M.M., Pabba, S., Safir, A., Cohn, R.W.: Visual force sensing with flexible nanowire buckling springs. Nanotechnology **19**, 035502 (2008)

25. Hsin, C.L., Mai, W.J., Gu, Y.D., Gao, Y.F., Huang, C.T., Liu, Y.Z., Chen, L.J., Wang, Z.L.: Elastic properties and buckling of silicon nanowires. Adv. Mater. **20**, 3919–3923 (2008)
26. Olsson, P.A.T., Park, H.S.: Atomistic study of the buckling of gold nanowires. Acta Mater. **59**, 3883–3894 (2011)
27. Ji, L.W., Young, S.J., Fang, T.H., Liu, C.H.: Buckling characterization of vertical ZnO nanowires using nanoindentation. Appl. Phys. Lett. **90**, 033109 (2007)
28. Young, S.J., Ji, L.W., Chang, S.J., Fang, T.H., Hsueh, T.J., Meen, T.H., Chen, I.C.: Nanoscale mechanical characteristics of vertical ZnO nanowires grown on ZnO:Ga/glass templates. Nanotechnology **18**, 225603 (2007)
29. Wen, Y.H., Wang, Q., Liew, K.M., Zhu, Z.Z.: Compressive mechanical behavior of Au nanowires. Phys. Lett. A **374**, 2949–2952 (2010)
30. Wang, G.F., Feng, X.Q.: Surface effects on buckling of nanowires under uniaxial compression. Appl. Phys. Lett. **94**, 141913 (2009)
31. Wang, G.F., Feng, X.Q.: Timoshenko beam model for buckling and vibration of nanowires with surface effects. J. Phys. D: Appl. Phys. **42**, 155411 (2009)
32. Yao, H.Y., Yun, G.H.: The effect of nonuniform surface elasticity on buckling of ZnO nanowires. Phys. E **44**, 1916–1919 (2012)
33. Challamel, N., Elishakoff, E.: Surface stress effects may induce softening: Euler–Bernoulli and Timoshenko buckling solutions. Phys. E **44**, 1862–1867 (2012)
34. Juntarasaid, C., Pulngern, T., Chucheepsakul, S.: Bending and buckling of nanowires including the effects of surface stress and nonlocal elasticity. Phys. E **46**, 68–76 (2012)
35. Wang, Y., Song, J.Z., Xiao, J.L.: Surface effects on in-plane buckling of nanowires on elastomeric substrates. J. Phys. D: Appl. Phys. **46**, 125309 (2013)
36. Liu, C., Rajapakse, R.K.N.D., Phani, A.S.: Finite element modeling of beams with surface energy effects. ASME J. Appl. Mech. **78**, 031014 (2011)
37. Miller, R.E., Shenoy, V.B.: Size-dependent elastic properties of nanosized structural elements. Nanotechnology **11**, 139–147 (2000)
38. Shenoy, V.B.: Atomistic calculations of elastic properties of metallic fcc crystal surfaces. Phys. Rev. B **71**, 094104 (2005)
39. Mi, C.W., Jun, S., Kouris, D.A., Kim, S.Y.: Atomistic calculations of interface elastic properties in noncoherent metallic bilayers. Phys. Rev. B **77**, 075425 (2008)
40. Chen, S.H., Yao, Y.: Elastic theory of nanomaterials based on surface energy density. ASME J. Appl. Mech. **81**, 121002 (2014)
41. Yao, Y., Wei, Y.C., Chen, S.H.: Size effect of the surface energy density of nanoparticles. Surf. Sci. **636**, 19–24 (2015)
42. Yao, Y., Chen, S.H.: Surface effect in the bending of nanowires. (2015) (Under review)
43. Yao, Y., Chen, S.H.: Surface effect on resonant properties of nanowires predicted by an elastic theory for nanomaterials. J. Appl. Phys. **118**, 044303 (2015)
44. Zhang, C., Yao, Y., Chen, S.H.: Size-dependent surface energy density of typically fcc metallic nanomaterials. Comput. Mater. Sci. **82**, 372–377 (2014)
45. Nix, W.D., Gao, H.: An atomic interpretation of interface stress. Scr. Mater. **39**, 1653–1661 (1998)
46. Sun, C.Q.: Oxidation electronics: bond–band–barrier correlation and its applications. Prog. Mater. Sci. **48**, 521–685 (2003)
47. Huang, Z.P., Wang, J.: A theory of hyperelasticity of multi-phase media with surface/interface energy effect. Acta Mech. **182**, 195–210 (2006)
48. Timoshenko, S.P., Gere, J.M.: Mechanics of Materials. Van Nostrand Reinhold Co., New York (1972)
49. Zhang, W.X., Wang, T.J., Chen, X.: Effect of surface/interface stress on the plastic deformation of nanoporous materials and nanocomposites. Int. J. Plast. **26**, 957–975 (2010)
50. Chen, T.Y., Chiu, M.S.: Effects of higher-order interface stresses on the elastic states of two-dimensional composites. Mech. Mater. **43**, 212–221 (2011)
51. Sheng, H.W., Kramer, M.J., Cadien, A., Fujita, T., Chen, M.W.: Highly optimized embedded-atom-method potentials for fourteen fcc metals. Phys. Rev. B **83**, 134118 (2011)
52. Diao, J.K., Gall, K., Dunn, M.L.: Atomistic simulation of the structure and elastic properties of gold nanowires. J. Mech. Phys. Solids **52**, 1935–1962 (2004)
53. Weinberger, C.R., Jennings, A.T., Kang, K.W., Greer, J.R.: Atomistic simulations and continuum modeling of dislocation nucleation and strength in gold nanowires. J. Mech. Phys. Solids **60**, 84–103 (2012)